Experimental and Numerical Study on the Gravitational Deposition and Coagulation of Aerosols

Huiyu Yu, Haifeng Gu*, Zhongning Sun, Yanmin Zhou, Junyan Chen and Yingzhi Li

Nuclear Power Plant Institute, Harbin Engineering University, Harbin, China

The gravitational deposition and coagulation of aerosols were studied experimentally based on the COSTTHES (Containment Source-Term and Thermal Hydraulics Experiment System) facility and numerically investigated based on a continuous general dynamic equation; the experimental and the numerical results were in good agreement. In the present study, the applicability of the zero-dimensional model for deposition and coagulation of aerosols was verified. A considerable distortion can occur due to the coagulation of the aerosol, which significantly influenced the removal rate of the aerosol with a diameter greater than 0.76 μm, and the dynamic shape factor value of the aerosol used in the present experiment was obtained as 4. In the experimental and numerical studies, it was found that the combined effect of the gravitational deposition and coagulation of the aerosol can increase the number density of the aerosol with specific diameters, and the concentration-increment size would increase as settling continued.

Keywords: gravitational deposition, coagulation, COSTTHES, GDE, aerosol

INTRODUCTION

Aerosol is one of the matter of concerns in the area of nuclear safety. During the course of a severe accident of a Pressurized Water Reactor (PWR), aerosols might be released from the ruptures of the coolant loop or generated from the Molten Core—Concrete Interaction (MCCI) (Sevón, 2005), and water vapor can be generated in the containment building, which causes the increase in pressure and temperature. Once the containment is breached, the radioactive aerosol will be released, which leads to a severe threat to the environment and the public. The radioactivity and the health hazard of the potential leakage are related to the concentration and size of the aerosol, and the time evolution of the aerosol concentration and the size distribution is influenced by various mechanisms. It is therefore of great importance to investigate the time evolution of the aerosol concentration and the size distribution of the aerosol.

The natural removal mechanisms (gravitational deposition, Brownian diffusion, thermophoresis settling, and diffusiophoresis settling) dominate aerosol size distribution and aerosol concentration in the absence of a spray system (Powers et al., 1996). In addition to the aforementioned settling mechanisms, coagulation affects the behavior of aerosol as well (Kwon and Lee, 2002). Though the coagulation does not result in the change in the mass of the aerosol in the containment, it influences the Particle Size Distribution (PSD) of the aerosol and then influences the overall removal efficiency of the aerosol (Schnell et al., 2006). The zero-dimensional Continuous General Dynamic Equation (Continuous GDE) is the commonly used numerical model to describe the settling and coagulation behavior of the aerosol (Friendlander, 2000). Many methods were developed to solve the GDE: the moment method (Zurita-Gotor and Rosner, 2004; Xie, 2014; Yu et al., 2015), the direct simulation

Monte Carlo (DSMC) method (Sheng and Shen, 2006; Sheng and Shen, 2007), the and sectional treatment method (Hounslow et al., 1988; Lister et al., 1995; Kumar and Ramkrishna, 1996; Geng et al., 2013). The moment method suffers from the shortcoming that a priori knowledge of the mathematical form of the size distribution of the aerosol is required; however, the experimental data provided by the instrument usually deviate more or less from the perfect mathematical form. As to the DSMC, its computation is expensive if the number of aerosol particles is large. In the settling process, the continuous decay of the particle number leads to a decrease in the simulation accuracy of the DSMC (Sheng and Shen, 2006).

Numerical studies related to the gravitational deposition and coagulation of the aerosol were conducted to analyze the behavior of the aerosol settling and coagulation. Lindauer and Castleman (1970) numerically studied the relative importance of Brownian and gravitational coagulation on the transient behavior of aerosol undergoing coagulation and gravitational settling. In his study, the homogeneous dispersed aerosol particles were assumed to be spherical. Powers et al. (1996) established a numerical model in which the settling mechanisms and coagulation mechanisms of aerosol were considered. In their study, it was indicated that the coagulation of the aerosol particles could lead to fantastic distortion from spherical, and the distortion of the aerosol agglomerate was considered by employing the dynamic shape factor. Garcia-Nieto (2006) numerically studied the scavenging efficiencies of aerosol emissions from coal-fired power plants; in the model, the coagulation and settling of aerosol were considered and the aerosol was considered as spherical particles, and it was found that the respirable dust has the lowest scavenging efficiency. Ghosh et al. (2017) developed a numerical model based on a semi-implicit solved GDE method, and it was revealed that the charge could significantly enhance the coagulation process of the aerosol. The model was validated against the results obtained by the experiment which was conducted in a $0.5m^3$ volume vessel. Recently, Narayanam et al. (2021) analyzed the growth and coagulation characteristics of the suspended sodium combustion aerosols in a closed chamber using the HAARM-S code which was based on the moment method; in their evaluation, the maximum error was around 50%.
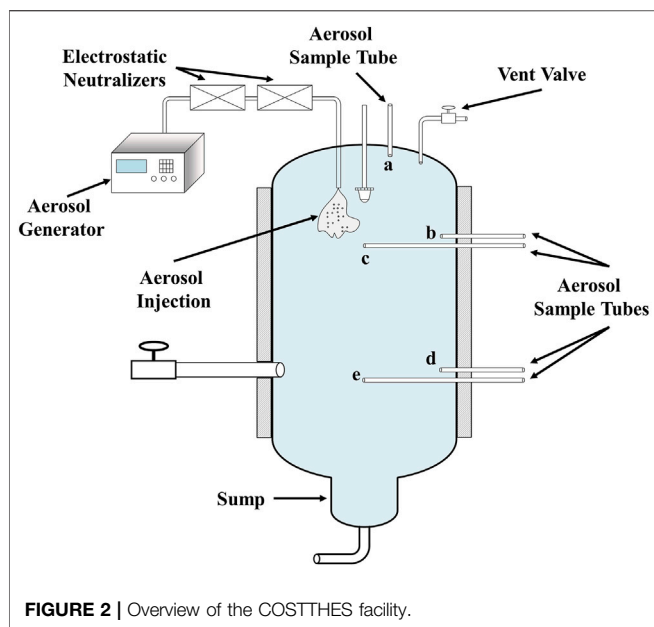
Kwon and Lee (2002) investigated separately the gravitational deposition and coagulation of aerosol using a horizontal cylinder and vertical cylinder; the experimental facility structure and its scale ensured the homogeneous distribution of the aerosol, that is, the potential stratification of the aerosol concentration was eliminated. The discussion of effective time in this study implied that the stratification of the aerosol concentration could occur under a static condition. The characteristics of the size evolution and the deposition velocity of the aerosol were studied experimentally by Kumar et al. (2015) (Subramanian et al., 2011; Misra et al., 2013; Kumar et al., 2015), and the experiments were conducted based on the ATF facility which had a closed chamber of $1m^3$ volume. Liu et al. (2017) conducted an experimental and numerical study on the decay of aerosol under high-concentration conditions and found that the wall-loss correction was valid when the initial concentration of the

FIGURE 1 | Vessel of the COSTTHES facility.

aerosol was less than $10^4 cm^{-3}$. The experimental study was conducted based on a stainless-steel cylinder container with a height of $0.55m$ and a volume of $0.54m^3$. In this numerical study, the aerosol was assumed to be a spherical particle and, hence, the dynamic shape factor was not considered. Freitag et al. (2018) investigated experimentally the wash-down of the aerosol due to the condensation of steam on the vertical wall of the containment; the experiment was conducted in the large-scaled THAI facility and the experimental results were compared with the COCOSYS calculations. Tian et al. (2020) investigated the characteristics of the natural deposition of aerosol using an enclosed vessel. The characteristics of the influences of the aerosol concentration and the static electricity on the deposition of the aerosol were investigated experimentally based on a cuboid vessel made of Plexiglass; the vessel had a height of $1.5m$ and a volume of $1.5m^3$. In the above numerical studies, most numerical models did not consider the influence of the dynamic shape factor of the aerosol, and the applicability of the zero-dimensional numerical model was not verified in a large-scaled container under a static condition. In the experimental studies of Liu, Kumar, and Tian, the small-scaled experimental facility minimized the influence of the stratification of aerosol concentration. However, the small scale of the experimental facility might amplify the influence of gas extraction due to sampling, which therefore might introduce additional errors.

In the present work, the combined effect of aerosol coagulation and gravitational deposition was studied experimentally based on

FIGURE 2 | Overview of the COSTTHES facility.

TABLE 1 | The configuration of the sample positions.

Sample notation	Height (m)	Distance from the wall (m)	Sampling zone
a	3.98	0.32	Up
b	3.09	0.2	Middle
c	3.09	1.0	Middle
d	0.71	0.2	Down
e	0.71	1.0	Down

the COSTTHES (Containment Source-Term and Thermal Hydraulics Experiment System) facility. The multisampling configuration (three sampling elevations) and the dimensions of the COSTTHES facility (a vessel with a height of $4.3m$ and a volume of $13.5m^3$) were made for the observation of the stratification of aerosol concentration and weakened the influence of the gas extraction due to sampling. In addition to the experiment, numerical analysis was conducted as well based on the continuous GDE considering the dynamic shape factor. Hence, the applicability of the zero-dimensional numerical model can be investigated under the condition in which the stratification of aerosol concentration can occur and the influence of the dynamic shape factor of the aerosol can be investigated.

EXPERIMENTAL FACILITY AND METHOD

Experimental Facility

The experimental study in the present work was conducted based on the COSTTHES facility. The facility and schematic of COSTTHES are shown in **Figure 1** and **Figure 2**

The COSTTHES facility is composed of a closed cylindrical vessel ($13.5m^3$ volume, $4.3m$ high, and $2m$ internal diameter). The aerosol generated from a PALAS RBG 2000D aerosol generator traveled through two electrostatic neutralizers to minimize the effect of static electricity before being injected into the vessel from the dome. Five sample tubes at different heights and radial positions were employed to obtain the aerosol spatial distribution, and the sampled aerosol was analyzed using a Welas Promo 3000H particle size spectrometer which has high precision, a wide measurement range (0.1–10 μm of aerosol diameter), and is capable of online sampling under high-pressure and high-temperature conditions. The configurations of the sample positions shown in **Figure 2** are listed in **Table 1**.

Experimental Procedure

In the experiment, as dried and filtered air was blown into the vessel to remove the water vapor and environmental aerosols, the humidity in the vessel was close to zero. While the air was transmitted, the vessel permitted the gas discharge to remain at atmospheric pressure; therefore, the pressure in the vessel was $1.01 \times 10^5 Pa$ and the temperature was 25°C. Then, the TiO_2 aerosol particles with an initial geometric mean diameter of $0.41\mu m$ and an initial geometric standard deviation of 1.32 were injected into the vessel. In the process of aerosol injection, the electrostatic neutralizers were kept in operation to ensure that the aerosol was not charged. The aerosol injection continued until the total number density of the aerosol was over $10^4/cm^3$ to manifest the influence of aerosol coagulation (Hussein et al., 2009; Yu et al., 2013; Liu et al., 2017). When the total number density of the aerosol reached the desired level, the aerosol generator was shut down but the feeding gas was still on for a few minutes to mix the aerosol inside the vessel. After the mixing step of the aerosol, the first sampling was carried out for 1 min to obtain the initial distribution of the aerosol; then all the valves of the vessel were shut down for hours to isolate the gas and aerosol inside the vessel from that of the environment. In the sampling process, the aerosol was extracted with the air in the vessel using a particle size spectrometer (Welas Promo 3000H) and the aerosols with different diameters were counted to obtain the size distribution of the aerosol. By switching the connection between the particle size spectrometer and the sample tube, the spatial distribution of the aerosol could be built. Considering the impact of gas extraction due to aerosol sampling, the sample operation was carried out discontinuously. The sampling flow rate at each sample position was controlled at $5L$/min and each sampling continued for 1 min, so that every sampling resulted in air extraction less than $25L$ compared with the COSTTHES vessel volume of $13.5m^3$.

An experiment was conducted to investigate the radial distribution of aerosol and the results are presented in **Figure 3**; it can be noted that the size spectra at the same height were adequately close to each before the aerosol was homogenous. Therefore, the experimental data acquired at the sampling positions c and e were employed to represent the size spectra at the corresponding heights. Because the aerosol was injected from the dome of the vessel, when the aerosol injection was just complete the number density at the higher position was much higher than that at the lower position, as shown in **Figure 4**. After 2.3 h of settling and mixing, the aerosol became almost
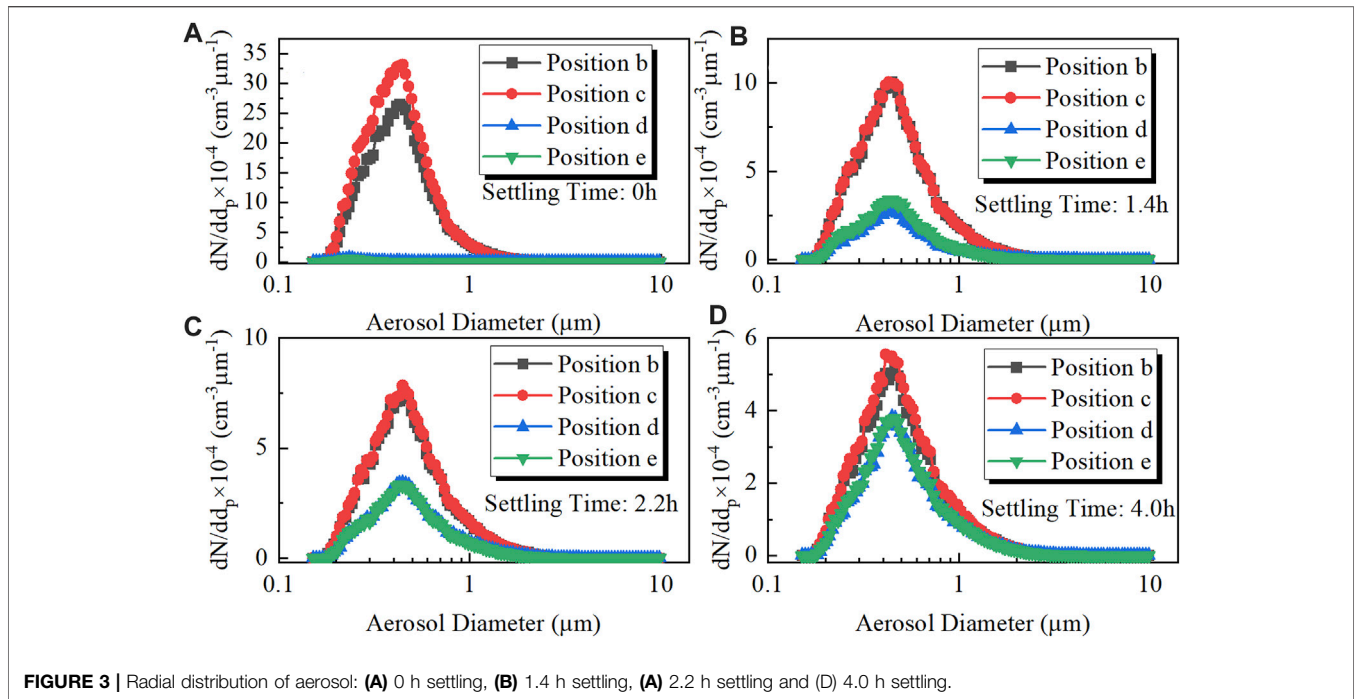
FIGURE 3 | Radial distribution of aerosol: **(A)** 0 h settling, **(B)** 1.4 h settling, **(A)** 2.2 h settling and (D) 4.0 h settling.
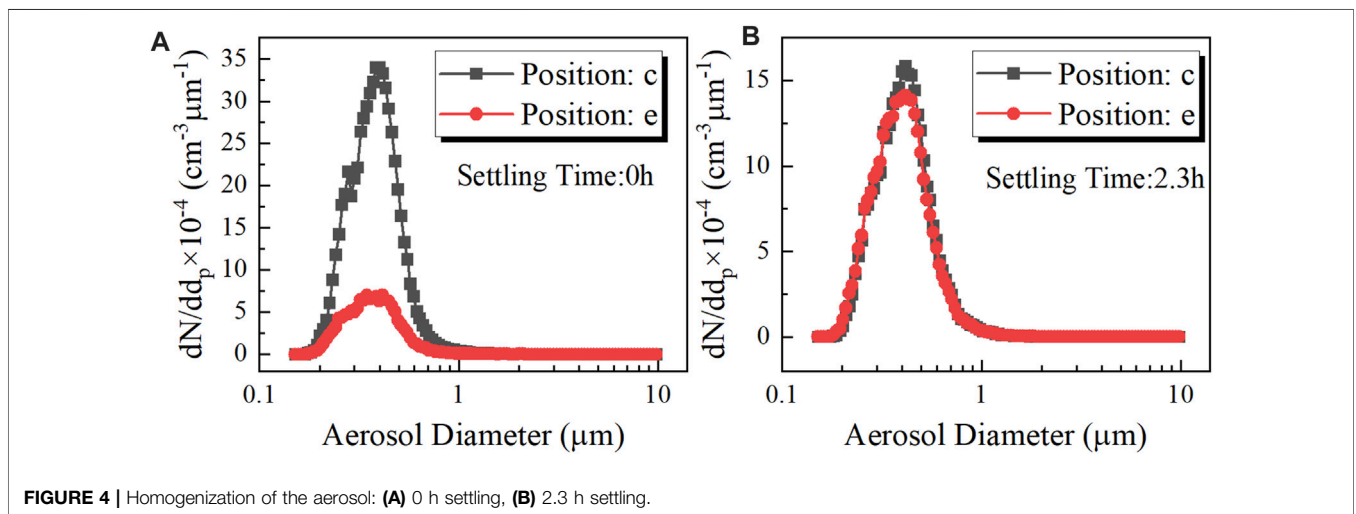

FIGURE 4 | Homogenization of the aerosol: **(A)** 0 h settling, **(B)** 2.3 h settling.

homogeneous in the vessel and the aerosol state at this moment and thereafter was used in the analysis.

COMPUTATION MODEL

General Dynamic Equation

In the present model, the aerosol spatial distribution was assumed to be homogeneous and the gravitational coagulation, Brownian coagulation, and gravitational deposition were considered the influencing mechanisms. Hence, the Continuous General Dynamic Equation (Continuous GDE) that governs the

aerosol kinetic behavior can be written in the following form (García-Nieto, 2001; García-Nieto, 2006; Kwon and Lee, 2002):

$$\frac{\partial n(v,t)}{\partial t} = \frac{1}{2} \int_0^v \beta(v-v',v') n(v-v',t) n(v',t) dv'$$
$$- n(v,t) \int_0^\infty \beta(v,v') n(v',t) dv' - \frac{v_g}{h} n(v,t) \quad (1)$$

where $n(v,t)$ (m^{-6}) is the number density of particles of volume v at a time t and represents the number of aerosols in unit spatial volume per unit aerosol volume, $\beta(v,v')$ is the coagulation kernel which is used to predict the coagulation frequency between

particles of volumes v and v', v_g is the gravitational deposition velocity, and h is the height of the vessel.

The first term on the right-hand side (RHS) of **Eq. 1** represents the rate of formation of particles between volumes v and $v + dv$ generated by coagulations between particles of volumes v and $v - v'$. The second term on the RHS stands for the death rate of particles of volumes between v and $v + dv$ due to coagulations with all other particles. The last term on the RHS represents the death rate of particles of volumes between volumes v and $v + dv$ due to gravitational deposition (Gelbard, 1982). The coagulation kernel can be written as (Powers et al., 1996)

$$\beta = \beta_G + (1 + 9/8\alpha^{2/3})\beta_B \qquad (2)$$

where β_G is the kernel of gravitational coagulation (Kwon and Lee, 2002), β_B is the kernel of Brownian coagulation (Kwon and Lee, 2002), and

$$\alpha = \frac{4\pi}{3kT}\rho_p g v_1^{1/3} v_2^{1/3} \left| v_1^{2/3} - v_2^{2/3} \right| \left(\frac{3}{4\pi} \right)^{4/3} \qquad (3)$$

where v_1 and v_2 denote the volumes of particles involved in the coagulation.

$$\beta_G = K_1 \varepsilon \left\{ (r_1 + r_2)^2 \left| r_1^2 - r_2^2 \right| + C_m \lambda (r_1 + r_2)^2 |r_1 - r_2| \right\} \qquad (4)$$

where $K_1 = 2\pi\rho_p g/9\mu$, $\varepsilon = 3y_c^2/2(r_1 + r_2)^2$, y_c is the minimum between r_1 and r_2, with r_1 and r_2 being the radii of the particles involved in the coagulation, C_m is the Cunningham slip correction factor, $C_m = 1 + \frac{2\lambda}{d_p}(1.257 + 0.4\exp(-1.1d_p/2\lambda))$, and λ is the mean free path of an air molecule.

$$\beta_B = K_2 (r_1 + r_2) \left\{ \left(\frac{1}{r_1} + \frac{1}{r_2} \right) + C_m\lambda \left(\frac{1}{r_1^2} + \frac{1}{r_2^2} \right) \right\} \qquad (5)$$

where $K_2 = 2kT/3\mu$.

Discretization of the General Dynamic Equation

The form of the nonlinear integro-partial-differential equation of the GDE makes the analytical solution rarely tractable. The widely used moment method can be used to determine the solution of the GDE with a low computation time; nevertheless, it does not permit variation in the resolution of the size distribution due to the fixed number of parameters (Lister et al., 1995). Moreover, in the moment method, one needs to assume the form of the initial size distribution of the particle, such as log-normal distribution for aerosols. However, the size distribution of the aerosol obtained with an instrument (e.g., a particle size spectrometer) usually does not perfectly fit the ideal log-normal distribution. Hence, the sectional treatment of the aerosol size distribution introduced by Lister et al. (1995) was used in the present model. In Lister's discretization scheme, the size distribution of the aerosol is divided into a finite number of sections (groups) and the ratio of volumes of two adjacent sections is $2^{1/q}$; therefore,

$$\frac{v_{i+1}}{v_i} = 2^{1/q} \qquad (6)$$

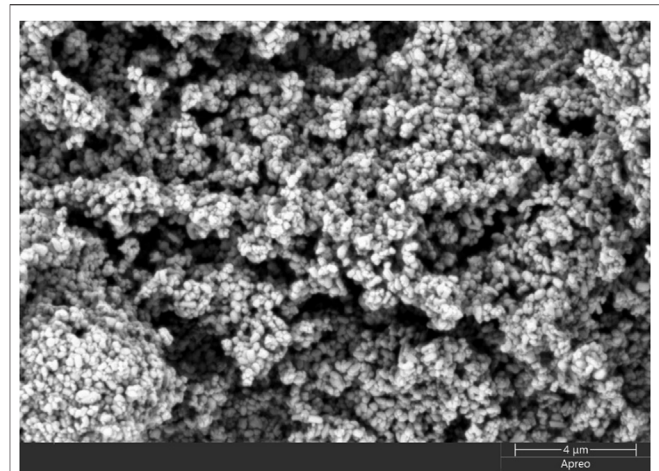where i is the index of the section and q is a positive integer constant.

FIGURE 5 | SEM image of the aerosol employed in the present study.

According to Lister's discretization scheme, **Eq. 1** can be transformed into

$$
\frac{dN_i}{dt} = \sum_{j=1}^{i-S(q)-1} \beta_{i-1,j} N_{i-1} N_j \frac{2^{(j-i+1)/q}}{2^{1/q}-1}
$$

$$
+ \sum_{k=2}^{q} \sum_{j=i-S(q-k+2)-k+1}^{i-S(q-k+1)-k} \beta_{i-k,j} N_{i-k} N_j \frac{2^{(j-i+1)/q}-1+2^{-(k-1)/q}}{2^{1/q}-1}
$$

$$
+ \frac{1}{2}\beta_{i-q,i-q} N_{i-q}^2
$$

$$
+ \sum_{k=2}^{q} \sum_{j=i-S(q-k+2)-k+2}^{i-S(q-k+1)-k+1} \beta_{i-k+1,j} N_{i-k+1} N_j \frac{-2^{(j-i)/q}+2^{1/q}-2^{-(k-1)/q}}{2^{1/q}-1}
$$

$$
- \sum_{j=1}^{i-S(q)} \beta_{i,j} N_i N_j \frac{2^{(j-i)/q}}{2^{1/q}-1} - \sum_{j=i-S(q)+1}^{\infty} \beta_{i,j} N_i N_j - \frac{v_g}{h}N_i
$$

$$\qquad (7)$$

where $N_i = \int_{v_i}^{v_{i+1}} n(v,t)dv$, $S(q) = \sum_{p=1}^{q} p$, and

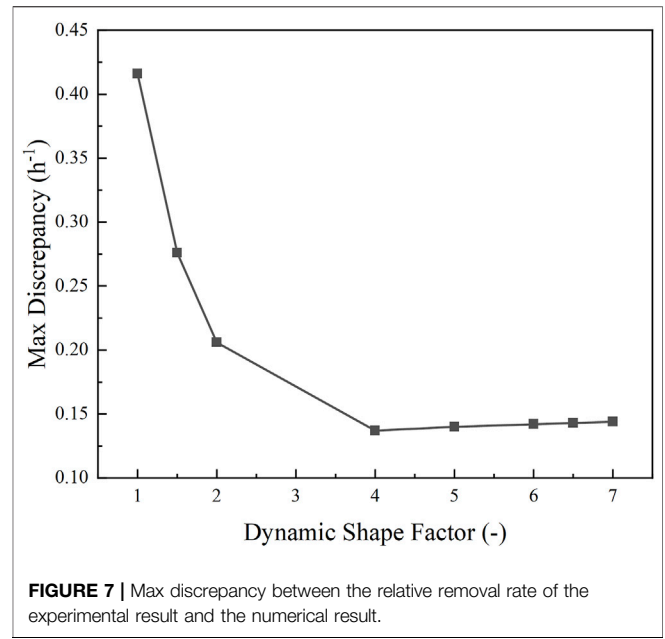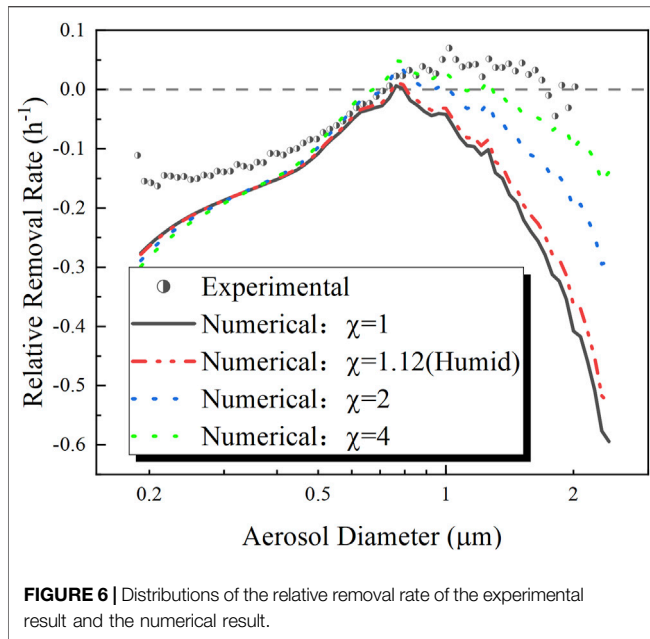$$v_g = \rho_p d_p^2 g C_m / 18\mu_g \chi \qquad (8)$$

where χ is the dynamic shape factor of the aerosol.

The accuracy and the resolution of the discretized size distribution of the aerosol increase with the increasing value of q. When $q = 6$, **Eq. 7** can be sufficiently precisely solved (Lister et al., 1995). **Equation 7** is a first-order linear ordinary differential equation and was solved using the finite-difference method in the present model.

EXPERIMENTAL RESULTS AND ANALYSIS

Dynamic Shape Factor

The sedimentation velocity of the aerosol particle is related to the dynamic shape factor of the aerosol, the diameter of the

FIGURE 6 | Distributions of the relative removal rate of the experimental result and the numerical result.

FIGURE 7 | Max discrepancy between the relative removal rate of the experimental result and the numerical result.

aerosol, the viscosity of air, and the density of the aerosol. The dynamic shape factor χ is defined as the ratio of the drag force experienced by a non-spherical particle to that experienced by a volume-equivalent spherical particle traveling at the same velocity in the same medium (Lau and Chuah, 2013). Hence, the dynamic shape factor is one of the important parameters influencing the sedimentation velocity of the aerosol of the non-spherical aerosol particle or coagulation that occurred. The primary particle of the aerosol employed in the present experiment was nearly spherical, as shown in **Figure 5**. However, the coagulation can generate significant distortions from spherical, which makes the dynamic shape factor greater than 1. In a humid environment such as the containment under a severe reactor accident, the surface tension effects produced by vapor condensation can reduce the dynamic shape factor (Powers et al., 1996). The dynamic shape factor in the humid environment can be calculated by $\chi = [\epsilon \rho_p + (1 - \epsilon)\rho_w]/\rho_p$, where ϵ is the packing fraction and is suggested to be 0.63 (Powers et al., 1996); then, the value of the dynamic shape factor was 1.12 for the aerosol material of TiO_2. Since the present experiment was conducted under dry air conditions, the dynamic shape factor was believed to be greater than 1.12 (humid conditions).

The removal constant defined by **Eq. 9** was usually used to evaluate the settling process of the aerosol. However, when the deposition is combined with coagulation of the aerosol, the removal constant might not be a constant throughout the settling process. Hence, in the present study, the relative removal rate was defined by **Eq. 10** and employed to analyze the settling process of the aerosol.

$$\lambda_i = \frac{dN_i}{N_i dt} \tag{9}$$

$$\bar{\lambda}_i = \frac{\int_0^{T_{sett}} \lambda_i(t)dt}{T_{sett}} \tag{10}$$

where T_{sett} is the settling time in the experiment.

The comparison between the relative removal rate of the experimental result and that of the numerical result is shown in **Figure 6**. It can be noticed that the numerical relative removal rate was approaching the experimental one for the aerosol with a diameter greater than 0.76 μm as the dynamic shape factor of the aerosol increased. According to **Eq. 8**, the gravitational deposition velocity of the aerosol particle decreases with increasing dynamic shape factor. Therefore, the gravitational deposition dominates the removal rate of TiO_2, an aerosol particle with a diameter greater than 0.76 μm.

The max discrepancies between the experimental distribution of the relative removal rate and the numerical ones with different dynamic shape factors are shown in **Figure 7** which indicates that the value of the dynamic shape factor is 4 in the present experiment.

Stratification of Aerosol Concentration

In the light of the above analysis, the dynamic shape factor in the present numerical study was set to 4, and the size distribution of the aerosol of the experimental result and that of the numerical result are compared in **Figure 8**. The comparison indicated that the experimental result and the numerical prediction were in good agreement.

Under the action of the gravitational deposition, the number density of the aerosol continuously decreased, as shown in **Figure 9** and **Figure 10**. As shown in **Figure 10**, the total number density of the aerosol increased with decreasing height; in other words, the stratification of the
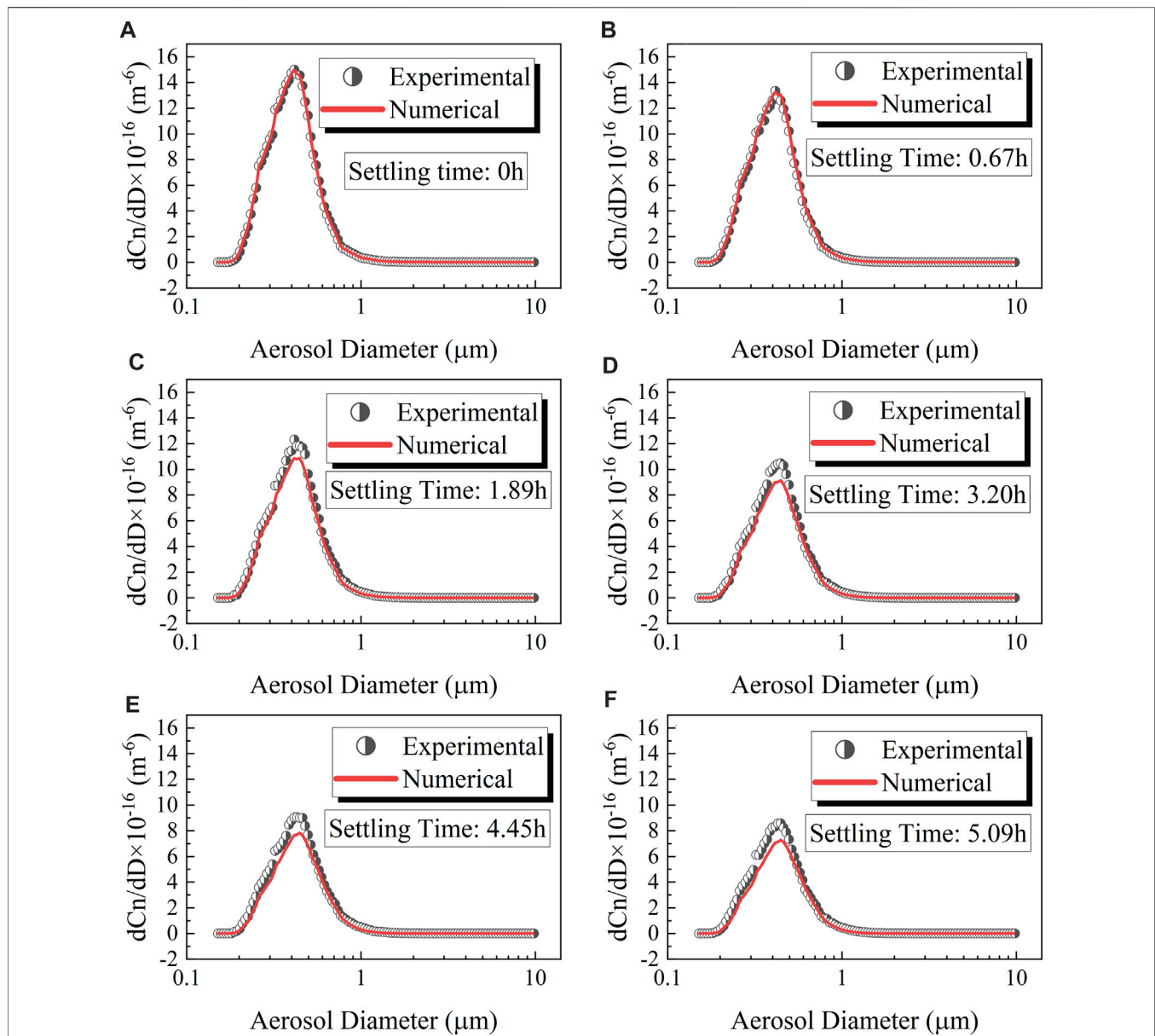
FIGURE 8 | Comparison of the experimental and numerical size distribution of the aerosol at different time, the dynamic shape factor x = 4: **(A)** 0 h, **(B)** 0.67 h, **(C)** 1.89 h, **(D)** 3.20 h, **(E)** 4.45 h and **(F)** 5.09 h.

aerosol concentration could be observed. However, in **Figure 9**, the median diameter of the aerosol did not appear stratified like the number density. As shown in **Figure 10**, the largest difference in the total number density of the aerosol in the Up Zone and the Down Zone was observed to be 9.5% at 3.2 h, and the largest prediction error with respect to the average total number density of the aerosol was 8.4% at 3.8 h. Hence, in 5.1 h of aerosol settling the stratification did not significantly affect the applicability of the zero-dimensional numerical model (GDE).

In the coagulation process, small particles aggregate into larger particles, which leads to an increase in the number density of the large particles. Nevertheless, the deposition of the large particle is much stronger than that of the small particles, which, on the contrary, results in a decrease in the number density of the large particles. In the present experiment, the median diameter of the aerosol particles increased throughout the duration of aerosol settling, as shown in **Figure 11**, which indicated that the coagulation mechanism is stronger than the deposition mechanism in the total number density range of the present experiment $(3.0 \times 10^4/cm^3$–$4.7 \times 10^4/cm^3)$. In the settling of the aerosol, though the median diameter of the aerosol kept increasing, the growth trend was slowing down, which indicated that the coagulation mechanism was weakening compared with the gravitational deposition.
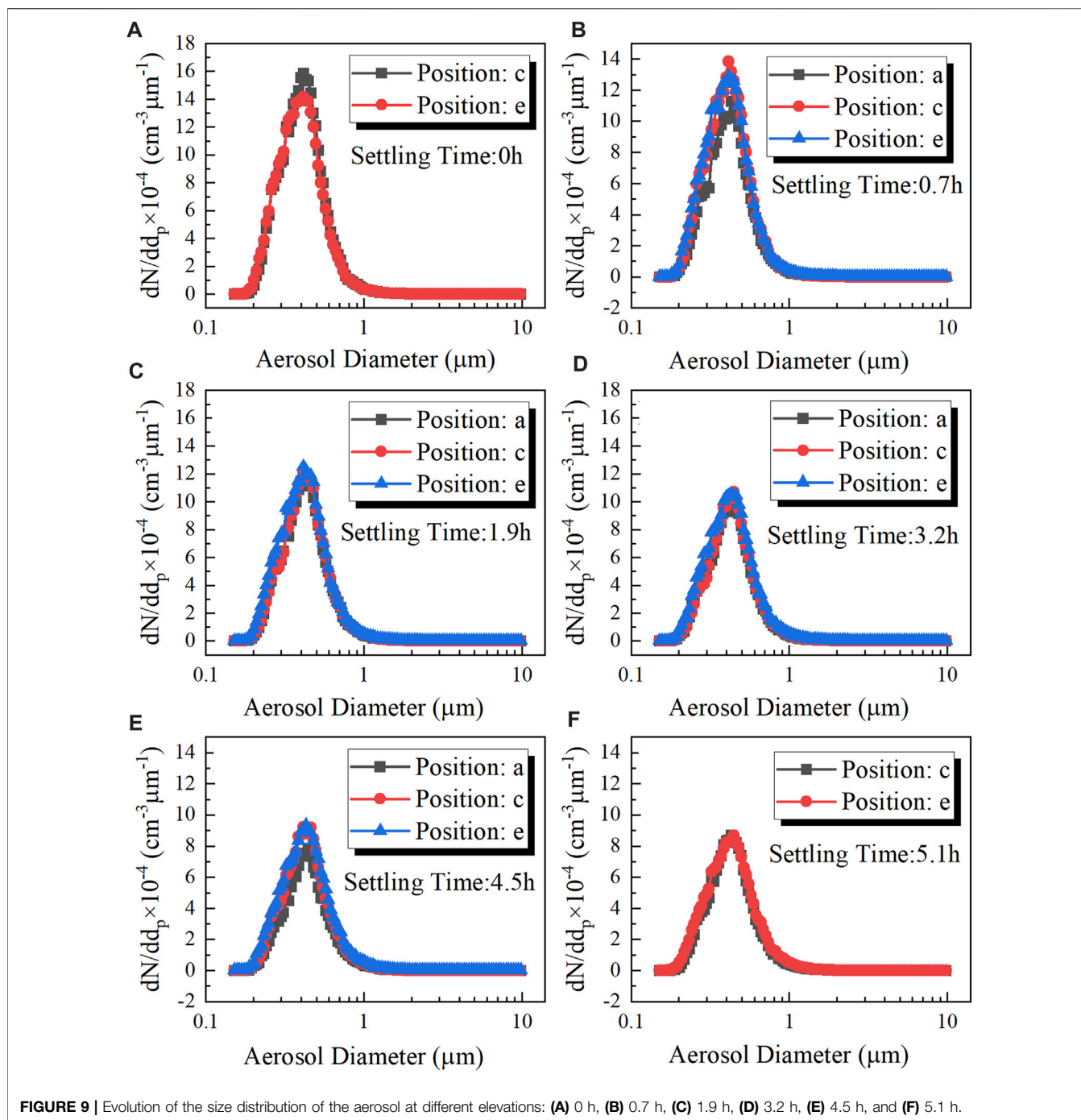
FIGURE 9 | Evolution of the size distribution of the aerosol at different elevations: **(A)** 0 h, **(B)** 0.7 h, **(C)** 1.9 h, **(D)** 3.2 h, **(E)** 4.5 h, and **(F)** 5.1 h.

Concentration-Increment Size

In order to analyze separately the influences of different mechanisms considered in the numerical model, the relative removal rate due to coagulation and gravitational deposition was calculated and is shown in **Figure 12**. According to **Eq. 7**, **Eq. 8**, and **Eq. 10**, the gravitational deposition is not affected by the number density of the aerosol, and the relative removal rate due to gravitational deposition did not vary with the settling time. However, the absolute value of the relative removal rate due to coagulation of the aerosol decreased with settling time, which is

attributed to the decreasing collision frequency due to the decreasing number density of the aerosol.

In the experimental result (**Figure 6**) and numerical result (**Figure 12**), a concentration increment phenomenon was observed. For the tiny aerosol (diameter below 0.6 μm), the relative removal rate was negative because of the predominant coagulation mechanism. For the large aerosol (diameter above 1.1 μm), the relative removal rate was negative as well because of the predominant gravitational deposition mechanism. However, the two aforementioned mechanisms were both weak for the medium
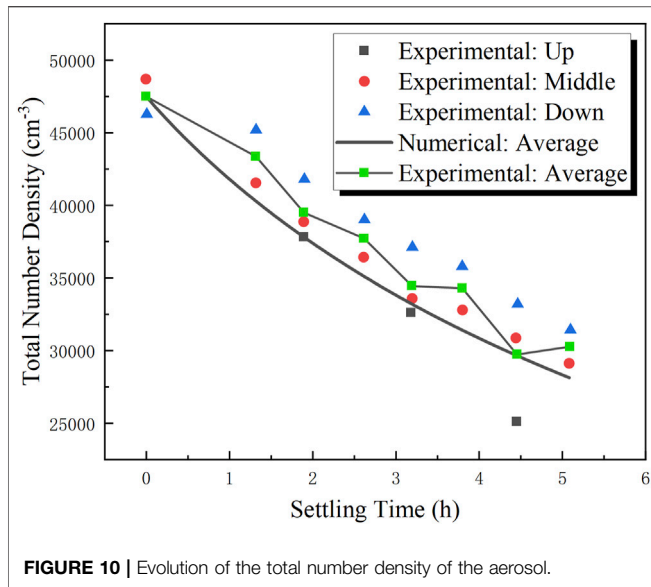
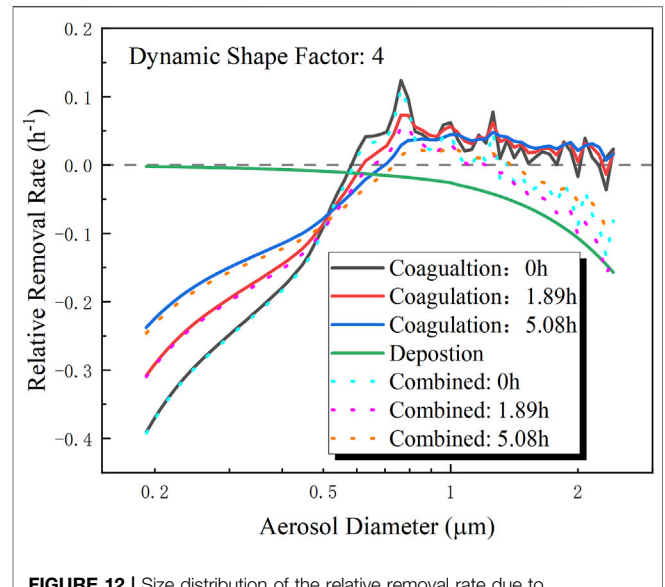**FIGURE 10 |** Evolution of the total number density of the aerosol.

FIGURE 12 | Size distribution of the relative removal rate due to gravitational deposition and coagulation.
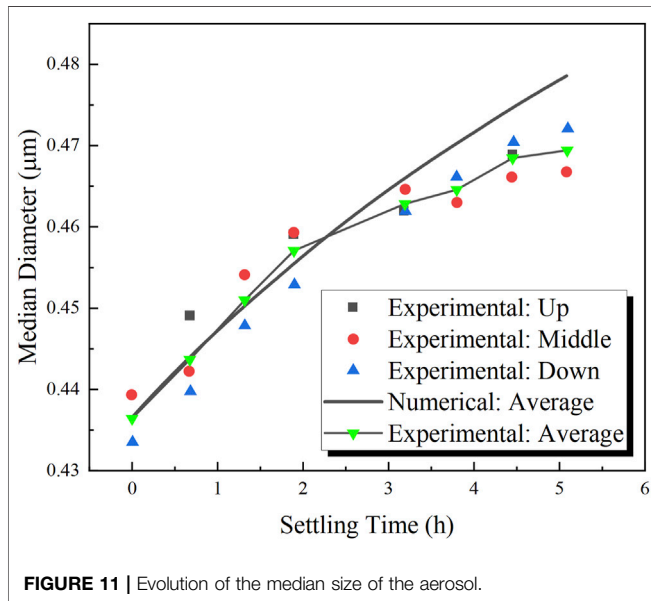

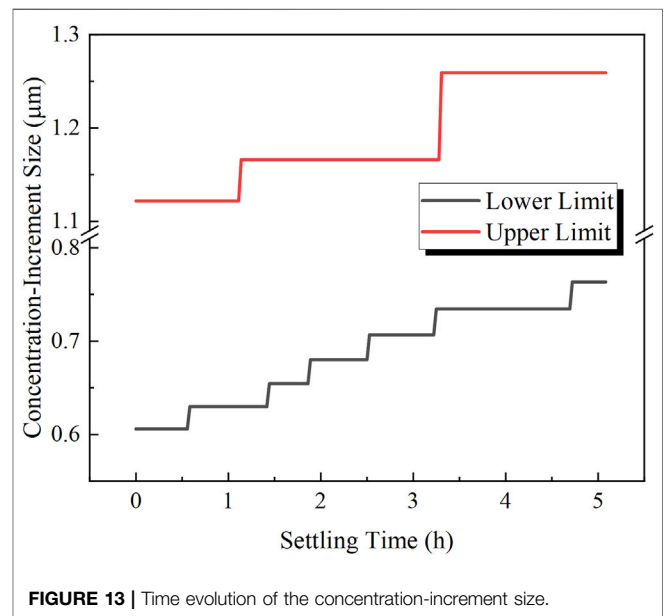**FIGURE 11 |** Evolution of the median size of the aerosol.

FIGURE 13 | Time evolution of the concentration-increment size.

size aerosol (diameter between 0.6 and 1.1 μm), which led to a positive relative removal rate (that is, the number density increased in a period). The time evolution of the concentration-increment size range is shown in **Figure 13**, within 5.1 h of settling; the lower limit of the concentration-increment size range was increased from 0.61 to 0.76 μm and the upper limit increased from 1.12 to 1.26 μm. Hence, as the gravitational deposition and coagulation continued, the concentration-increment size increased.

CONCLUSION

The gravitational deposition and coagulation are significant phenomena for the aerosol in the severe reactor accident. In

this study, the gravitational deposition and coagulation were studied experimentally based on the COSTTHES facility and numerically with the population balance method. According to the present experimental and numerical studies, we draw the following conclusions: 1) The comparison between the experimental results and the numerical results showed that the present numerical model could predict the deposition and coagulation behavior of the aerosol with a satisfying agreement. 2) The experimental results and the numerical predictions showed that the behavior of the aerosol with a diameter greater than 0.76 μm was dominated by the gravitational deposition

mechanism, which was influenced significantly by the dynamic shape factor, and, in the present experiment, the dynamic shape factor was inferred to be 4. 3) The stratification of aerosol concentration was observed in the experiment; the largest difference in the total number density of the aerosol at different elevations was observed to be 9.5%, and the largest prediction error was 8.4%. Hence, the zero-dimensional numerical model was still applicable within 5.1 h of settling though the aerosol concentration stratification existed. 4) In the present experiment, the median diameter of the aerosol kept growing within 5.1 h of settling, which indicated that gravitational deposition was the predominant mechanism compared with coagulation. The slowing down growth trend of the median diameter of the aerosol indicated the weakening coagulation mechanism due to the decreasing number density of the aerosol. 5) A concentration increment phenomenon was observed in the experiment and predicted by the numerical model during aerosol settling, and it was found that as the gravitational deposition and coagulation continued the concentration increment size increased.

REFERENCES

Friendlander, S. K. (2000). *Smoke, Dust and Haze: Fundamentals of Aerosol Dynamics*. New York, USA: Oxford University Press. 38-2208-38-2208. doi:10.5860/choice.38-2208

Freitag, M., Gupta, S., Beck, S., and Sonnenkalb, M. (2018). Experimental and Analytical Investigations of Aerosol Processes—Wash-Out and Wash-Down. *Nucl. Sci. Eng.* 193, 198–210. doi:10.1080/00295639.2018.1479091

García-Nieto, P. J. (2001). Parametric Study of Selective Removal of Atmospheric Aerosol by Coagulation, Condensation and Gravitational Settling. *Int. J. Environ. Health Res.* 11, 149–160. doi:10.1080/09603120020047528

García-Nieto, P. J. (2006). Study of the Evolution of Aerosol Emissions from Coal-Fired Power Plants Due to Coagulation, Condensation, and Gravitational Settling and Health Impact. *J. Environ. Manag.* 79, 372–382. doi:10.1016/j.jenvman.2005.08.006

Gelbard, F. (1982). *MAEROS User manual.[LMFBR]*. Albuquerque, NM (USA): Sandia National Labs.

Geng, J., Park, H., and Sajo, E. (2013). Simulation of Aerosol Coagulation and Deposition under Multiple Flow Regimes with Arbitrary Computational Precision. *Aerosol Sci. Technol.* 47, 530–542. doi:10.1080/02786826.2013.770126

Ghosh, K., Tripathi, S. N., Joshi, M., Mayya, Y. S., Khan, A., and Sapra, B. K. (2017). Modeling Studies on Coagulation of Charged Particles and Comparison with Experiments. *J. Aerosol Sci.* 105, 35–47. doi:10.1016/j.jaerosci.2016.11.019

Hounslow, M. J., Ryall, R. L., and Marshall, V. R. (1988). A Discretized Population Balance for Nucleation, Growth, and Aggregation. *AIChE J.* 34, 1821–1832. doi:10.1002/aic.690341108

Hussein, T., Hruška, A., Dohányosová, P., Džumbová, L., Hemerka, J., Kulmala, M., et al. (2009). Deposition Rates on Smooth Surfaces and Coagulation of Aerosol Particles inside a Test Chamber. *Atmos. Environ.* 43, 905–914. doi:10.1016/j.atmosenv.2008.10.059

Kumar, A., Subramanian, V., Baskaran, R., and Venkatraman, B. (2015). Size Evolution of Sodium Combustion Aerosol with Various Rh. *Aerosol Air Qual. Res.* 15, 2270–2276. doi:10.4209/aaqr.2015.03.0150

Kumar, S., and Ramkrishna, D. (1996). On the Solution of Population Balance Equations by Discretization-I. A Fixed Pivot Technique. *Chem. Eng. Sci.* 51, 1311–1332. doi:10.1016/0009-2509(96)88489-2

Kwon, S. B., and Lee, K. W. (2002). Experimental and Numerical Study of Aerosol Coagulation by Gravitation. *Part. Part. Syst. Charact.* 19, 103–110. doi:10.1002/1521-4117(200205)19:2<103::AID-PPSC103>3.0.CO;2-I

Lau, R., and Chuah, H. K. L. (2013). Dynamic Shape Factor for Particles of Various Shapes in the Intermediate Settling Regime. *Adv. Powder Technol.* 24, 306–310. doi:10.1016/j.apt.2012.08.001

Lindauer, G. C., and Castleman, A. W. (1970). The Importance of Gravitational Coagulation on the Settling of High-Mass Density Aerosols. *Nucl. Sci. Eng.* 42, 58–63. doi:10.13182/nse70-a19327

Lister, J. D., Smit, D. J., and Hounslow, M. J. (1995). Adjustable Discretized Population Balance for Growth and Aggregation. *AIChE J.* 41, 591–603. doi:10.1002/aic.690410317

Liu, L., Zhang, Z., Wu, Y., Yang, W., Wu, S., and Zhang, L. (2017). Decay of High-Concentration Aerosol in a Chamber. *Aerosol Sci. Eng.* 1, 155–159. doi:10.1007/s41810-017-0015-z

Misra, J., Subramanian, V., Kumar, A., Baskaran, R., and Venkatraman, B. (2013). Investigation of Aerosol Mass and Number Deposition Velocity in a Closed Chamber. *Aerosol Air Qual. Res.* 13, 680–688. doi:10.4209/aaqr.2012.06.0159

Narayanam, S. P., Kumar, A., Pujala, U., Subramanian, V., Srinivas, C. V., Venkatesan, R., et al. (2021). Theoretical Simulation on Evolution of Suspended Sodium Combustion Aerosols Characteristics in a Closed Chamber. *Nucl. Eng. Technol.* 0–6. doi:10.1016/j.net.2021.12.029

Powers, D. A., Washington, K. E., Burson, S. B., and Sprung, J. L. (1996). *A Simplified Model of Aerosol Removal by Natural Processes in Reactor Containment*. U.S. Nucl. Regul. Comm. Albuquerque USA: (NRC), NUREG-CR-6173.

Schnell, M., Cheung, C. S., and Leung, C. W. (2006). Investigation on the Coagulation and Deposition of Combustion Particles in an Enclosed Chamber with and without Stirring. *J. Aerosol Sci.* 37, 1581–1595. doi:10.1016/j.jaerosci.2006.06.001

Sévón, T. (2005). *Molten Core-Concrete Interactions in Nuclear Accidents: Theory and Design of an Experimental Facility*. Helsinki, Finland: VTT Technical Research Centre of Finland.

Sheng, C., and Shen, X. (2006). Modelling of Acoustic Agglomeration Processes Using the Direct Simulation Monte Carlo Method. *J. Aerosol Sci.* 37, 16–36. doi:10.1016/j.jaerosci.2005.03.004

Sheng, C., and Shen, X. (2007). Simulation of Acoustic Agglomeration Processes of Poly-Disperse Solid Particles. *Aerosol Sci. Technol.* 41, 1–13. doi:10.1080/02786820601009704

Subramanian, V., Baskaran, R., Misra, J., and Indira, R. (2011). Experimental Study on the Behavior of Suspended Aerosols of Sodium and Nonradioactive Fission Products (SrO2 and CeO2) in a Closed Vessel. *Nucl. Technol.* 176, 83–92. doi:10.13182/NT11-A12544

Tian, L. T., Gu, H., Yu, H., and Chen, J. (2020). Experimental Study on the Natural Deposition Characteristics of Erosols in Containment. *Front. Energy Res.* 8, 345. doi:10.3389/fenrg.2020.527598

Xie, M.-L. (2014). Asymptotic Behavior of TEMOM Model for Particle Population Balance Equation over the Entire Particle Size Regimes. *J. Aerosol Sci.* 67, 157–165. doi:10.1016/j.jaerosci.2013.10.001

Yu, M., Koivisto, A. J., Hämeri, K., Seipenbusch, M., and Hämeri, K. (2013). Size Dependence of the Ratio of Aerosol Coagulation to Deposition Rates

DATA AVAILABILITY STATEMENT

The original contributions presented in the study are included in the article/Supplementary Material; further inquiries can be directed to the corresponding author.

AUTHOR CONTRIBUTIONS

YH contributed to the conception and design and data analysis of the study. GH, SZ, and ZY provided guidance and suggestions for the study. CJ and LY assisted in the experiment.

FUNDING

for Indoor Aerosols. *Aerosol Sci. Technol.* 47, 427–434. doi:10.1080/02786826.2012.759640

Yu, M., Liu, Y., Lin, J., and Seipenbusch, M. (2015). Generalized TEMOM Scheme for Solving the Population Balance Equation. *Aerosol Sci. Technol.* 49, 1021–1036. doi:10.1080/02786826.2015.1093598

Zurita-Gotor, M., and Rosner, D. E. (2004). Aggregate Size Distribution Evolution for Brownian Coagulation-Sensitivity to an Improved Rate Constant. *J. Colloid Interface Sci.* 274, 502–514. doi:10.1016/j.jcis.2004.02.065

Conflict of Interest: The authors declare that the research was conducted in the absence of any commercial or financial relationships that could be construed as a potential conflict of interest.

Publisher's Note: All claims expressed in this article are solely those of the authors and do not necessarily represent those of their affiliated organizations, or those of the publisher, the editors, and the reviewers. Any product that may be evaluated in this article, or claim that may be made by its manufacturer, is not guaranteed or endorsed by the publisher.